LIFTING LINE METHOD FOR MODELLING COVERING AND BLANKETING EFFECTS FOR YACHT FLEET RACE SIMULATION

Thomas Spenkuch[1], ts305@soton.ac.uk
Dr. Stephen Turnock[2], srt@soton.ac.uk
Dr. Matteo Scarponi[3], ms1004@soton.ac.uk
Prof. Ajit Shenoi[4], r.a.shenoi@soton.ac.uk

Abstract. An approach is presented that can be used to enhance the realism of yacht fleet race simulations. The wake of an upwind sailing yacht is represented as a single heeled horseshoe vortex (and image) system. At each time step changes in vortex strength are convected into the wake as a pair of vortex line elements. These subsequently move in accordance with the local wind, self-induced velocity and velocity induced by the presence of the wakes of other yachts. An empirical based decay factor is used to eventually remove the far wake. A synthesis of sail yacht wake representations based on detailed 3D Reynolds Averaged Navier-Stokes (RANS) Computational Fluid Dynamics (CFD) calculations with wind tunnel test results are used to capture the initial strength of the combined main-jib vortex system and its vertical height. These were based on a typical upwind sail arrangement for a range of heel angles and in-line calculations for a pair of yachts separated by three boat lengths. This paper details the basis of the validated CFD results for a yacht at heel and the analysis of the CFD results to provide an approximate single line vortex method for the yacht. The developed algorithm will eventually run within the Robo-Race which is a real-time yacht race strategy analysis tool based on MATLAB®-Simulink® developed at the University of Southampton.

NOMENCLATURE

ACC	America's Cup Class
AoA	Angle of Attack
CFD	Computational Fluid Dynamics
RANS	Reynolds Averaged Navier-Stokes
SST	Shear Stress Transport
C_L, C_D	Lift and drag coefficients
L	Sail rig and yacht length
$\vec{r} = \{x, y, z\}$	Position
U	Freestream velocity
$\vec{q} = \{u, v, w\}$	Induced velocities in x-, y-, -z directions
Γ_i	Vortex strength of element i
ω	Vorticity

1. INTRODUCTION

The traditional way of quantifying the performance of a sailing yacht is carried out by assessing how fast a yacht will complete a course under given conditions. The *Robo-Race* simulator which allows both influence of the yacht design and tactical choices of the crew has been developed to capture the behaviour of a fleet of yachts [1, 2]. It is designed to simulate fleet races with *N* America's Cup Class yachts, where *M* yachts are controlled by the computer and *(N-M)* yacht are controlled by a real sailor. In these simulated regattas sailors can race against other yachts crewed by an Artificial Intelligence (AI) decision-making engine that has been created using a combination of structured interviews and questionnaires designed to identify expertise level based response. Different models for the yacht-crew interaction have been designed and implemented for the helmsman and the sail tailors, as well as a 'routing engine' which solves problems of a strategic and a tactical nature, such as collision avoidance and navigation in wind shifts.

As part of a fleet race simulation it is important to be able to capture the interactions between multiple yachts. The upwind sailing performance of a yacht is influenced by the presence of another yacht when the downwind yacht sails in the wind shadow of the upwind yacht. The upwind yacht is said to 'blanket' or 'cover' the downwind yacht. The blanketing effect is caused by the 'wash' of the sails of the upwind yacht which has an effect on the flow propagating downwind reducing its magnitude and altering its direction. Existing models such as [3] provide an empirical approach to the phenomenon of blanketing and this is the approach implemented in the current version of 'Robo-Race' [1, 2]. This model is based on 'wind shadow penalties' received by the trailing yacht when sailing upwind or by the leading yacht when sailing downwind. The penalty depends on factors such as the distance between the two yachts and their relative positions. Philpott *et al.* used two different approaches, according to the point of sail [3]. When the yacht disturbing the air sails upwind, a change of wind direction is assumed (*bent air effect*). Alternatively, when the yacht disturbing the flow sails downwind, wind speed reductions behind the yacht relative to the undisturbed airflow are assumed (*turbulent air effect*).

The increase in computational performance provides an opportunity to capture more of the flow complexity, especially for multiple yachts. The use of the vortex line element representation of a lifting surface can capture the alteration to flow direction and speed in an efficient manner. It is proposed that a yacht sail system be replaced by a single lifting line system. This work sets out to determine the appropriate shed vortex element

---
1 Research Student, Fluid Structure Interactions Research Group, School of Engineering Sciences, University of Southampton, UK
2 Reader, Fluid Structure Interactions Research Group, School of Engineering Sciences, University of Southampton, UK
3 Head of Group, Fluid Structure Interactions Research Group, School of Engineering Sciences, University of Southampton, UK
4 Research Engineer, Wolfson Unit for Marine Technology and Industrial Aerodynamics, University of Southampton, UK

strength at each time step and its initial vertical position. These quantities can be determined using a Reynolds Averaged Navier-Stokes (RANS) Computational Fluid Dynamics (CFD) calculations for an upwind sail arrangements.

CFD flow investigations are often used as part of the design process of high performance sailing yachts and are now a key component of elite racing yacht campaigns, such as the America's Cup or the Volvo Ocean Race [4, 5].

The examination of how well CFD predicts the performance of the sails against wind tunnel data was carried out in [6, 7]. These studies showed that the application of CFD solvers gave detailed information about the complex flow in the wake of a typical sail rig for a range of sailing conditions. The work presented introduces the 'Robo-Race' simulator, details the proposed lifting line approach, presents the results of a CFD study into the interaction between a pair of in-line upwind sailing yachts, and compares the behaviour of the lifting line model with the CFD approach.

2. THE SAILING SIMULATOR *ROBO-RACE*

The simulator Robo-Race is a MATLAB®-Simulink® based tool which is built on the module 'Robo-Yacht' which provides the yacht 'physics engine' as well as behavioural models for the automatic crew [1, 2] (Figure 1). This automatic crew consists of the following three members each given a specific task:

Helm:
- Modelled by proportional-integral-derivative (PID) controller
- Outputs the rudder angle and rudder rate
- Steers to a reference apparent wind angle or towards the next mark

Sail Tailor:
- Outputs are the sheeting angle and its derivative
- A PID controller minimises the error between the reference sheeting angle and its actual value
- A second controller depowers the sail to limit the actual heeling

Navigator:
- Checks the position of the yacht on the racecourse
- Issues strategic decisions
- Detects changes in wind conditions
- Controls manoeuvres and the following speed recovery

Robo-Race is a sailing simulator which takes into account the human factor with respect to strategic decisions during a fleet race. The simulator is designed in a way that one or more users (sailors) can interact with computer controlled yachts.
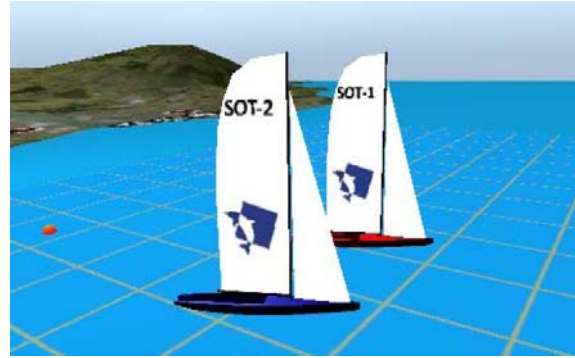

Figure 1. Virtual Environment in Robo-Race; two yachts on the race course [2].

This setup provides the recording, analysis, and comparison of the sailors' behaviour, strategies, tactics, and decision-making process. Different models for the yacht-crew interaction have been designed and implemented for the helmsman and the sail tailors, as well as a 'routing engine' which solves problems of a strategic and a tactical nature, such as collision avoidance and navigation in wind shifts. A virtual reality (VR) environment supports the sailor with a visual real-time feedback of the race state and of his/her yacht within a virtual 3D world. The user effects control through use of a steering wheel (helm) which controls the rudder angle directly, a joystick for changing the viewpoint, a 17" flat screen for displaying the onboard instruments and three projectors for displaying the 3D sailing environment on a cluster of screens (see Figure 2) [8].

Figure 2. Advanced Display Environment showing wheel and curved display panels for VR driven by 3 data projectors [8].

In order to simulate fleet races with *N* yachts, Robo-Race includes *M* Robo-Yachts which are controlled by the simulator and (*N-M*) human controlled yachts. In order to define a yacht-crew system the setup of the hull, rig and crew parameters for each Robo-Yacht are required. In addition, two further modules were implemented in order to enhance the realism of the simulation. Firstly, a weather module is used, which prescribes the spatial and temporal variation of the wind speed and direction. Secondly, a race scenario module has been implemented which deals with rule-based routing strategy and an additional library which achieves efficient race tactics and addresses conflicts between tactics and race strategy.

An example is tacking onto an unfavoured beat to sail in clean air that is not in the wake of a leading yacht.
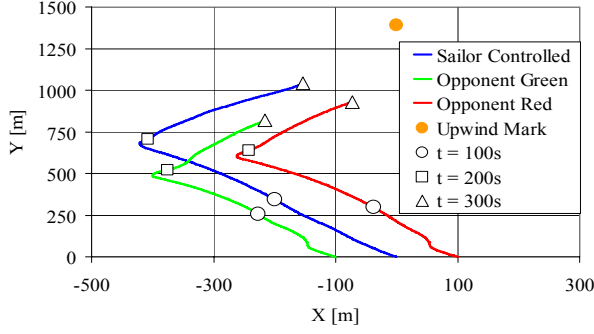

Figure 3. Example of race tracks and identification of position at three different times, as the two computer controlled yachts respond to the wind shifts. The pattern of wind variation can be seen in their course variation.

The *Physics Engine*, i.e. the yacht motion is modelled by a four degrees of freedom (DoF) model (surge, sway, yaw and roll) developed by Masuyama which has proven to perform well for tacking simulations in calm water as the obtained results were in good agreement with those of full scale experiments [9].

3. LIFTING LINE METHOD

A weakness of the current approach is in capturing the flow interactions between multiple yachts. It is proposed that the use of an appropriate series of vortex line elements can improve the representation of the modification to the local wind strength and direction due to the presence of multiple yachts. The challenge of developing such an approach is to ensure that it is robust and that it requires only a modest increase in computation at each time step. To deal with this challenge a lifting line approach based on [10] is used describing the physical phenomena of blanketing and covering.

At every time step, a vortex system with a vortex strength Γ_i is shed according to the actual lift generated by the sail rig. This vortex system consists of three nodes; one node NT_i (Node Top) generated at around 70% of the mainsail height and one node NB_i (Node Bottom) at the water surface. The third node represents the image of node NT_i and is referred to NTI_i (Node Top Image). The horizontal vortex elements created by two successive nodes NT_i and NT_{i-1} has the vortex strength Γ_{i-1}, whereas the vertical vortex element possesses the strength $\Delta\Gamma_i$ calculated by the difference of Γ_i and Γ_{i-1} (see Figure 4). In order to describe the natural flow behaviour and to assure a robust and computational model, a linear decay rate in time is superimposed to the vortex strength along the filaments.

$$\frac{d\Gamma}{dt} = K \cdot \frac{\Gamma_{initial}}{t} \qquad (1),$$

where K is a constant.

For this analysis, a node with its vortex element will be deleted if its corresponding vortex strength drops below 5% of its initial shed value. Thus, the induced velocities at each node due to the presence of the other vortex elements are calculated and the nodes' displacements are determined. Note that this approach also considers the influence of close-by yachts on the vortex elements. At the end of a routine step, the nodes' locations are updated, and the influence of the local wind induced drift is also taken into account.
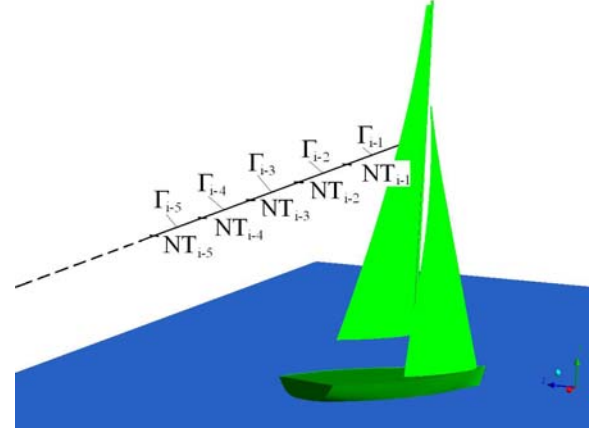

Figure 4. Nomenclature used for the lifting line model describing the vortex system of a sailing yacht, Nodes Top (NT_i) and corresponding vortex strength Γ_i (Top Nodes are shown).

The induced velocity $d\vec{q}$ of a vortex filament of strength Γ and a length of dl can be calculated with the Biot-Savart law

$$d\vec{q} = \frac{\Gamma\left(d\vec{l} \times \vec{r}\right)}{4\pi r^3} \qquad (1).$$

Rewritten in scalar form, the magnitude of the induced velocity is

$$dq = \frac{\Gamma \sin\theta dl}{4\pi r^2} \qquad (2).$$

Using the following substitutions, where

$$l = \|N_2 - N_1\| \qquad (3)$$

is a segment with the vorticity vector pointed from Nodes N_1 to N_2 and P is a point in space whose normal distance to the line joining N_1 to N_2 is r_P. Hence

$$r = \frac{r_P}{\sin\theta} \quad (4), \qquad dl = r_P\left(\frac{1}{\sin^2\theta}\right)d\theta \quad (5),$$

and integrating between N_1 and N_2 gives the magnitude of the induced velocity as

$$q_{\theta_{12}} = \frac{\Gamma}{4\pi r_P}\int_{\theta_1}^{\theta_2}\sin\theta d\theta = \frac{\Gamma}{4\pi r_P}\left(\cos\theta_1 - \cos\theta_2\right) \quad (6),$$

where θ_1 and θ_2 are the two orientation angles shown in Figure 5.

From referring Figure 5, the following terms can be stated:

$$r_P = \frac{|\vec{r}_1 \times \vec{r}_2|}{r_0} \quad (7), \qquad \cos\theta_1 = \frac{\vec{r}_0 \cdot \vec{r}_1}{r_0 r_1} \quad (8),$$

$$\cos\theta_2 = \frac{\vec{r}_0 \cdot \vec{r}_2}{r_0 r_2} \quad (9),$$

where r expresses the magnitude of the vector $\vec{r}$.
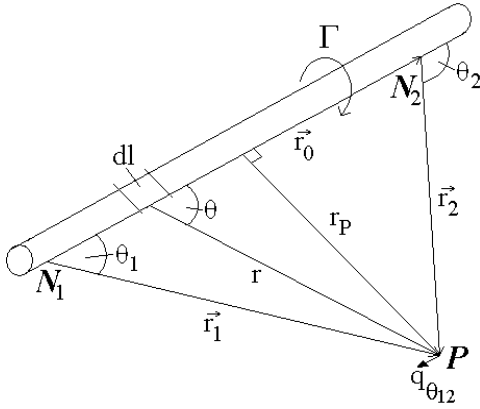
Figure 5. Nomenclature of the distances and angles for the vortex-induced velocity calculation at a point P [10].

Substituting these expressions into Equation (6) and knowing that the direction of the induced velocity is given by the unit vector

$$\frac{\vec{r}_1 \times \vec{r}_2}{|\vec{r}_1 \times \vec{r}_2|} \quad (10),$$

Equation (6) updates to

$$\vec{q}_{\theta_{12}} = \frac{\Gamma}{4\pi}\frac{\vec{r}_1 \times \vec{r}_2}{|\vec{r}_1 \times \vec{r}_2|^2}\left[\vec{r}_0 \cdot \left(\frac{\vec{r}_1}{r_1} - \frac{\vec{r}_2}{r_2}\right)\right] \quad (11).$$

Now the components of the induced velocity can be expressed as

$$u = Coef \cdot \left(r_1 \times r_2\right)_x \quad (12),$$

$$v = Coef \cdot \left(r_1 \times r_2\right)_y \quad (13),$$

$$w = Coef \cdot \left(r_1 \times r_2\right)_z \quad (14),$$

$$Coef = \frac{\Gamma}{4\pi|r_1 \times r_2|^2}\left(\frac{r_0 \cdot r_1}{r_1} - \frac{r_0 \cdot r_2}{r_2}\right) \quad (15).$$

4. CFD INVESTIGATIONS

A detailed examination of the performance of a typical upwind sail rig arrangement was carried out for different heel and yaw angles using a commercial CFD solver. Experimental wind tunnel data provided by the Wolfson Unit for Marine Technology and Industrial Aerodynamics were used to validate the calculated CFD results. A brief introduction and the CFD procedure adopted are explained below.

4.1   Sloop Rig Model

The Wolfson Unit for Marine Technology and Industrial Aerodynamics evaluated a sailing yacht at the University of Southampton in the low speed section of a wind tunnel (4.6m width by 3.7m height). The model was mounted on a six-component balance attached to a turntable and suspended from the balance in a tank of water [11]. Different sail setups and heel angles were tested. The experimental data obtained from these wind tunnel tests were used to carry out a validation study into the influence of heel upon the performance of a sloop rig (see Figure 6).

The dimensions for the jib and mainsail surfaces are defined by five sections beginning at the foot (0%) and increasing in steps of 25% up to the top (100%). Each sail section shape is defined by its camber, draft, and front and back percentage (see [6] for further information). The angle of the sail towards the mast angle varies for each section to create the span-wise distribution of the sail twist in order to model more realistic sailing conditions. The foot length of the jib and the mainsail are 774 mm and 667 mm respectively. The height of the jib is 1618 mm and the mainsail is 2000 mm high comprising a total sail area A made up of 0.665 m^2 (jib) and 0.720 m^2 (mainsail). Figure 6 shows the sail rig surfaces with a superimposed viscous grid of medium density.

The following 3D simulations with different incidence and heel angles are executed to determine the effect of heeled sails. The comparison with the experimental data shows the level of accuracy of the CFD calculations and gives an idea of the accuracy of the viscous wake analysis. The lift and drag coefficients of the sail rig are used for the validation and defined further below (see Equations 16 and 17).

For the viscous sail wake analysis, the criteria of maximum vorticity [12] and minimum pressure [13] are used for the identification of the position of the vortex cores. Different surfaces parallel to the inlet and outlet wall of the wind tunnel are introduced downstream of sail rig beginning at the stern of the yacht and continued by 0.5, 1.5, 3.5, 6, 9 yacht lengths behind it for the small domains and 12, 15, 18 yacht lengths for the big domain. On those surfaces the vorticity ω is calculated and defined as the curl of the velocity (see Equation 18):

$$Cl = \frac{Lift}{0.5\rho u_\infty^2 A} \quad (16), \qquad Cd = \frac{Drag}{0.5\rho u_\infty^2 A} \quad (17),$$

$$\vec{\omega} = \vec{\nabla} \times \vec{u} \qquad (18),$$

where A is the sail area of 1.385 m^2.

Two additional analysis surfaces are introduced 0.2 sail rig lengths upwind of the rig in order to determine the flow angle 'seen' by the rigs.

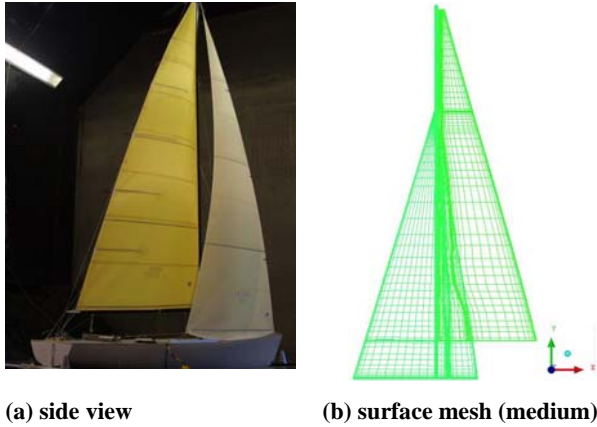**(a) side view**   **(b) surface mesh (medium)**

Figure 6. Views of experimental test (a) and corresponding computational sail rig mesh (b)

4.2 Initial Investigations and Setup

All meshes and simulations for this study were carried out using the software packages of ANSYS® ICEM CFD 11.0 and ANSYS® CFX 10.0. As stated in [14], the Shear Stress Transport (SST) offered the best performance for the available computational power and is the applied turbulence model for all calculations within this study, whereas the fluid air is set up as an ideal gas.

Wind tunnel tests on 2D impervious sails carried out by Newman and Low [15] were used to investigate three different mesh types (structured, unstructured and hybrid) at four different mesh densities around typical sail sections with the effect on lift, drag, reattachment and separation locations analysed. The similar Reynolds numbers of 1.2x10^5 (Newman and Low) and 1.71x10^5 (Wolfson Unit data) provide confidence that the flow conditions and behaviour are similar. Further 2D investigations using a cut of the sail rig at the height of 5% of the luff of the mainsail were carried out to determine an appropriate mesh technique, a time step value for the unsteady runs and the difference of the steady and unsteady simulation approach. The structured meshes utilised an H-block topology for each sail with features such as clustering at the leading/trailing edges, boundary layer mesh around the sails to ensure a y$^+$-value of 1 and an O-grid around the mast (see Figures 7 and 8). Detailed information about this mesh sensitivity study can be found in [6].

A structured 2D mesh of 163,900 cells was found to give an acceptable level of fidelity without requiring a too large a 3D mesh. The results of the 2D slice mesh sensitivity study were used to build a 3D mesh around the jib-mainsail-mast configuration.

Supplementary investigations into the boundary layer growth on the wind tunnel working section walls were made to find a method whereby these could be treated with a 'free-slip' condition and yet any axial pressure gradient effects could be captured.
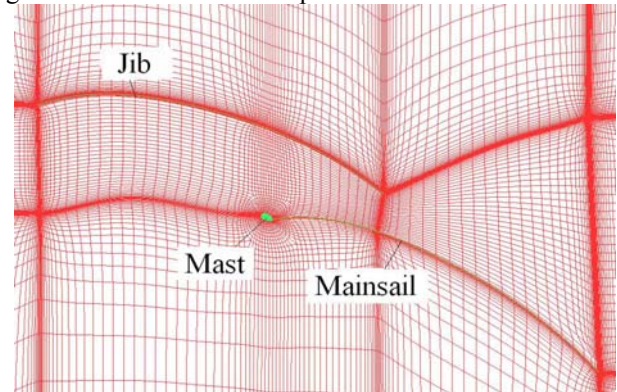

Figure 7. Smooth structured mesh of medium density

For the 3D simulations three structured meshes were chosen, consisting of the wind tunnel domain including the jib, the mainsail and the mast. The applied block topology offers the opportunity to split the blocks around the sail rig in such a way that an approximation to a rotary disc was created in order to adapt the mesh easily to the actual heel and wind incidence angles. The wind tunnel domain is split in 576 blocks; 6 in x-, 8 in y- and 12 in the z-direction. The large number of blocks is due to the need to split the domain 12 times in z-direction to assure that the blocks are correctly associated to the complex twisted sail rig structure. Three structured meshes with the same features as the 2D meshes described above were created for the grid validation investigation (see Table 1 and Figure 9).

The following boundary conditions are set up:
- velocity inlet at the wind tunnel inlet, pressure outlet at the wind tunnel outlet;
- no-slip wall condition at the jib, mainsail, mast, wind tunnel bottom; and
- free slip wall condition at the wind tunnel ceiling and side walls (the wind tunnel is reduced by the same amount of the boundary layer thickness on these walls in order to apply these saved cells around the sail rig).

Table 1. Mesh sensitivity study, individual C_D and C_L for the jib and mainsail. A practical restriction of 4 million cells limited further mesh sensitivity studies with finer meshes. 27° AoA and 0° heeled sail rig.

Grid Density	Number of Cells	Jib		Mainsail	
		C_D	C_L	C_D	C_L
Coarse	851,469	0.123	0.934	0.209	0.505
Medium	1,692,787	0.111	0.94	0.207	0.508
Fine	3,374,461	0.102	0.93	0.21	0.516

The velocity of the flow through the wind tunnel domain was 7 m/s which corresponds to a Reynolds Number of 1.71x10^5. Two different series of runs were carried out to

investigate the effect of the heeling angle and the angle of attack (AoA) on sailing performance. These were:

1. to investigate the influence of the angle of attack, the angle of attack varies whereas the heel angle remains constant (AoA varies in values of 23°, 27°, 32° and the heel angle is kept constant at 0°, 30°);
2. to investigate the influence of the heel angle, the heel angle varies whereas the angle of attack remains constant (AoA remains constant at 27° and the heel angle varies in values of 0°, 10°, 20°, 30°).
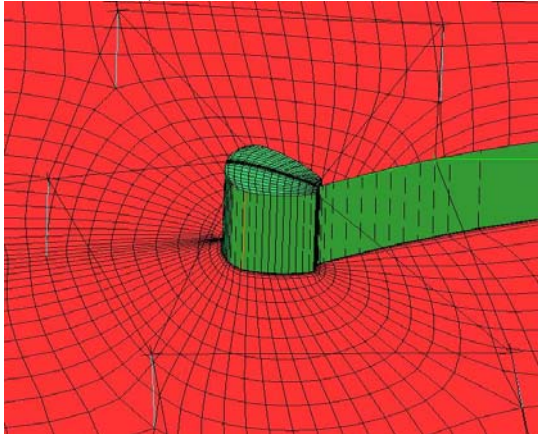
Figure 8. Smooth structured mesh of medium density with O-mesh around the mast (view at mast and mainsail)
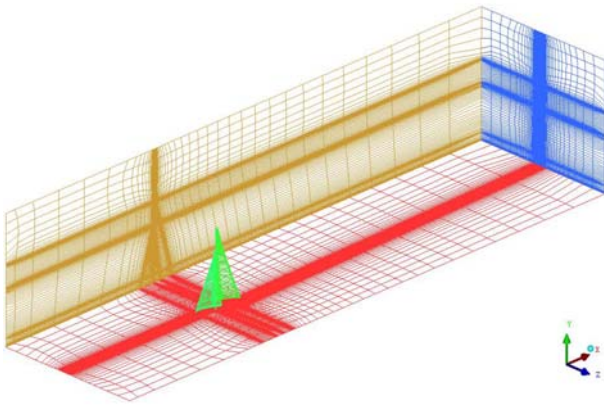
Figure 9. 3D wind tunnel domain mesh of middle density with sail rig located 3 sail rig lengths downstream of the inlet and 10 sail rig length upstream of the outlet

In order to complete the detailed wake analysis and to ensure that the size of the wind tunnel domain was sufficient, a larger domain was generated using 1.8 million cells (8.5 sail rig lengths width by 24 sail rig lengths by 2 sail rig lengths height).

Furthermore, to gain useful information for the evaluation of the lifting line model, a multiple fleet race environment is set up by using an extended wind tunnel domain with two sail rigs in-line and a distance of three sail rig lengths between the up and downwind yacht (2.5 million elements).
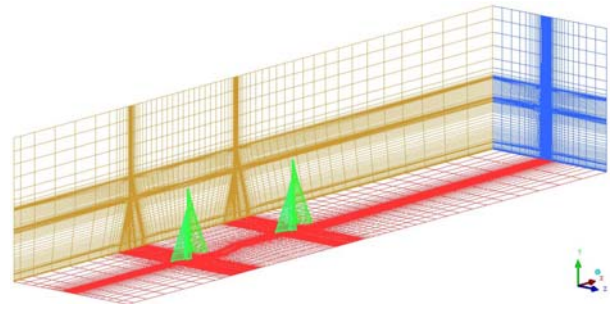

Figure 10. 3D wind tunnel domain mesh with 2 sail rigs in-line, whereas a distance of 3 sail rig lengths is implemented between the yachts.

4.3 CFD Results for one Yacht

Figure 11 shows the experimental and CFD results for a varying heel angle where the AoA is kept at a constant 27°. It can be seen that C_L and C_D decrease approximately linearly to a heel angle of 20° and increase for the 30° heeled sail rig. Fig. 11 illustrates the same development of the CFD and experimental data as the heel angle increases. It can be seen that CFD is able to capture the flow behaviour observed during the wind tunnel tests in the Wolfson Unit. Generally, an overprediction of the drag coefficient is observed which can be explained by: (1) a general overprediction of drag by the SST model with (2) the use of an insufficiently fine mesh of middle density due to the lack of computational power.
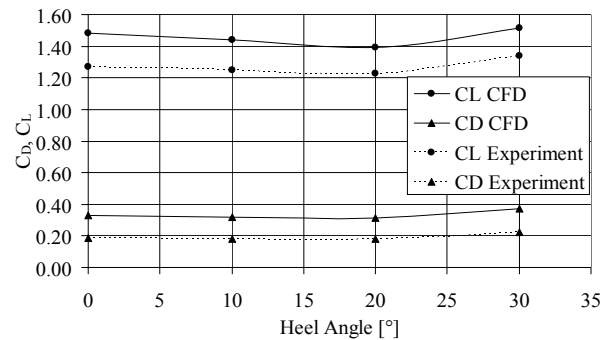

Figure 11. C_D and C_L for experimental data and CFD results. Different heel angles are investigated where the AoA remains constant at the value of 27°.

Figure 12 below displays the CFD results with and without the hull, and the experimental data of the Wolfson Unit. The presented experimental values are obtained by easing the position of the sails (de-powering of the sails) whereas the hull and the wind direction remained constant. The best fit lines describe the efficiency of the sail rig height where lines of shallow slope identify greater efficiency than the steep ones as their lift to drag ratio increases.
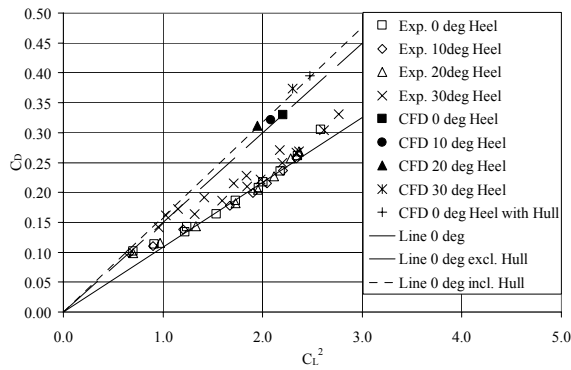
Figure 12. Experimental and CFD data for 27° AoA including hull

The added lines in Figure 15 above show a difference between the efficiency of the 0° and 30° heeled sails for the experimental results as the efficiency increases for the 30° heeled case. This can be viewed as a reduction in the induced drag for the heeled case [16]. The same behaviour is observed for the CFD results as the lines of best fit identify a loss of efficiency for the 30° heel angle compared to the 0° heel angle simulation. Furthermore, not only is the notable change of the shift in the lines captured by the CFD calculation, but also the fact that the three data points for 0°, 10° and 20° cases are comparable as can also be seen from the experimental results. The effect of the hull on the performance of the sailing yacht is also evident. The slope of the corresponding line is steeper than that of those without the hull. This loss of efficiency can be explained considering Figure 14, where a flow 'jump' over the hull is observed. This 'jump' makes the flow less efficient by changing the pressure distribution of the jib and mainsail in an unfavourable way, especially at the foot.
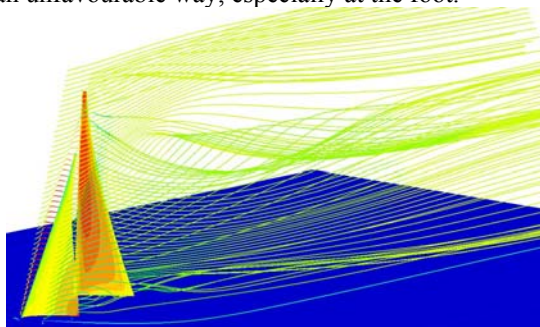

Figure 13. Local pressure contour on sails and streamlines to identify the vortices in the wake. 27° AoA and 10° heeled sail rig.

Three main vortices are generated by the sail rig; two smaller ones at the top of the mast and at the end of the foot of the mainsail and a large vortex around the top region of the jib and mainsail. The two smaller vortices decrease in strength rapidly and are almost negligible after 3-4 yacht lengths downstream of the sail rig.

This confirms the decision to restrict the vortex system per yacht to just one trailing vortex line was correct since the main vortex at a height close to that of

the jib effectively coalesces all of the shed vorticity within two yacht lengths (see Figures 13, 14 and 15).
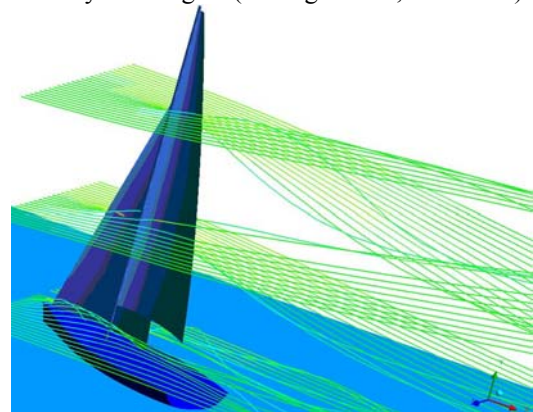

Figure 14. Streamlines around sailing yacht to show the updated flow behaviour downwind as the flow has to 'jump' over the hull. 27° AoA and 0° heel angle.
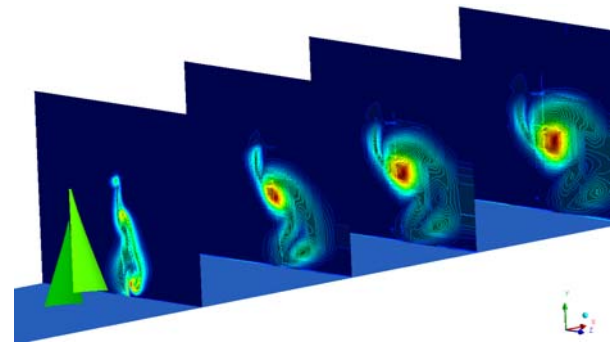

Figure 15. Vortex core development by showing the vorticity contour on surfaces downstream of the sail rig (varying local surface range).

4.4 CFD Results for two Yacht

The blanketing and covering effects on the downwind yacht due to the presence of the upwind yacht can be seen in Figure 16 and is also clearly visible on the sails' lift and drag coefficients. Table 2 displays the C_L and C_D values of the jibs and mainsails for the two yachts. The drag on the jib for the downwind yacht increases (plus 35%) whereas the lift decreases in value of 22%. For the mainsail both coefficients decrease in value, whereas the favourable decline of 11% for C_D is accompanied by a 22% loss in lift.

Table 3 shows the loss in performance for the downwind yacht by displaying the ratio of C_L to C_D. The individual sail ratio decreases in value by 43% for the jib and 12% for the mainsail and results in a combined loss for the sail rig of almost 36%. The presence of the upwind yacht alters the flow behaviour significantly whereas the flow angle 'seen' by the downwind yacht is changed by 9.95° considering the 'undisturbed' flow acting on the upwind rig. It should be noted that these values are not directly comparable to those in Table 1 due to the presence of the tunnel walls. Also, in an actual sailing environment the sailing conditions of the

downwind yacht would be adjusted. Nevertheless, the loss in performance is real.
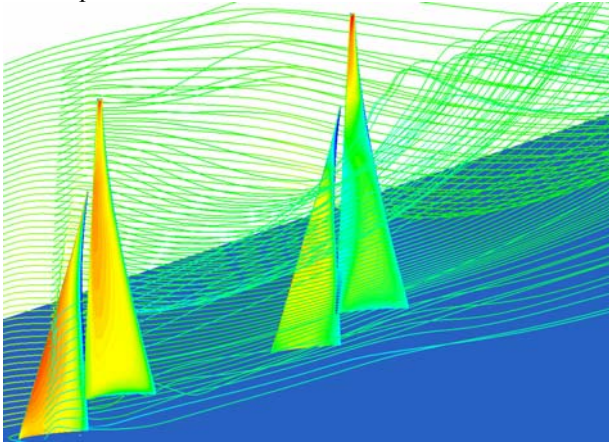

Figure 16. 3D wind tunnel domain mesh with two sail rigs in-line and a distance of 3 sail rig lengths. Varying local pressure contours on downwind sail rig due to the updated flow behaviour. Streamlines to identify the vortices (constant pressure range on both rigs).

Table 2. C_L and C_D values of the upwind and downwind sail rigs considering the individual sails.

	Jib		Mainsail	
	C_D	C_L	C_D	C_L
Upwind Yacht	0.122	1.038	0.214	0.525
Downwind Yacht	0.165	0.806	0.190	0.412
Difference [%]	35.39	-22.31	-11.01	-21.62

Table 3. Ratio of C_L and C_D of the upwind and downwind sail rigs considering the individual and combined sails.

	C_L/C_D		
	Jib	Mainsail	Combined
Upwind Yacht	8.539	2.459	5.499
Downwind Yacht	4.900	2.166	3.533
Difference	-42.62	-11.92	-35.76

5. EVALUATION AND RESULTS OF THE LIFITNG LINE METHOD

Figure 17 below displays the development of the maximum vorticity of the dominant vortex downstream of the sail rig. It can be observed that the vorticity values have different starting values and decrease exponentially. The varying vorticity starting values can be explained by the difference in sail lift which differs according to the actual incidence angle. The steep decrease in vortex strength continues up to the value of 2 yacht lengths downstream and decelerates thereafter. Furthermore, it can be seen that the exponential decrease in vortex strength (vorticity) does not vary much for the different sail rig setups and wind conditions. The simulation using the large (big) domain illustrates the development of the vortex strength further downstream and continues the exponential vorticity decrease of the smaller domain simulations.
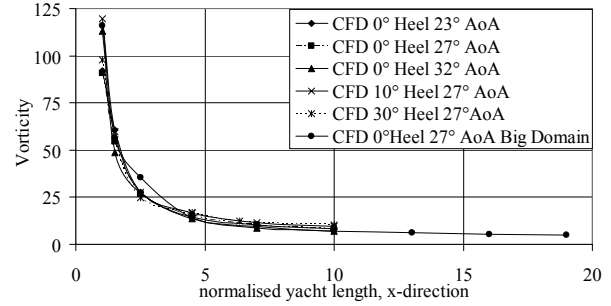

Figure 17. Vorticity development downstream of the sail rig, *0* in x-direction describes the bow and *1* the stern of the sailing yacht, CFD results for different heel and incidence angles using small and big domains.

Figure 18 shows the vertical and tangential tracks of the vortex cores at different locations downstream of the sail rig. It can be observed that the filaments of the vortex cores start at around 70% of the mainsail height, whereas the highest shed off value is reached at 32° AoA. Afterwards, the vortex core filaments decrease to a minimum that occurs at around 57% in vertical and 13% horizontal direction for all runs using the small domain expect for the 30 heeled sail rig setup (60% and 18%, respectively). Subsequently, the vortex cores gain between 3% and 5% in height, whereas the simulation with 32° AoA achieves the greatest increase.

Furthermore, the vortex core of the 30° heeled sail rig covers the greatest horizontal distance of all sail rig setups. The big domain simulation shows a slightly different behaviour as the vortex is less influenced by the wind tunnel side walls. The vortices have more space for their development and moves further away from the sail rig. Therefore, the location of the minimum is altered and occurs at around 30% in horizontal direction. Subsequently, the vortex cores increase in height and remain at a horizontal value of 67% for 12, 15 and 18 sail rig lengths downstream of the yacht. Moreover, an almost identical horizontal and vertical location of the vortex cores 15 and 18 sail rig lengths downstream can be observed.

For the lifting line method, the complexity of the whole wake flow field is represented by a series of line element vortices in order to generate the same velocity field as calculated from the CFD simulations. The vortex field is simulated by reproducing the predicted vortex core filament from the CFD calculations. This filament is divided into several elements on which a constant vortex strength Γ is implemented. The vortex strength Γ is calculated by using the total lift coefficient acting on the sail rig as:

$$\Gamma = \frac{k.C_L \cdot S \cdot U}{2h} \quad (19),$$

where h describes the height of the mainsail and k is a factor which accounts for the interaction between the main and jib vortex system. A similar formulation is used
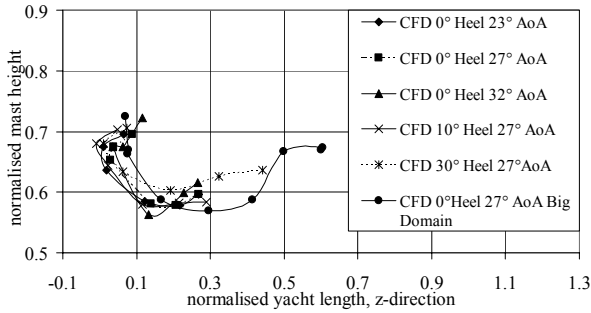
Figure 18. Vortex core tracks within the sail rig wake downstream; the line starting points begin at around 70% of the normalised mainsail height and describe the position of the vortex cores at the stern of the yacht.

by Roncin and Kobus [17] who investigated the interaction between two yachts by simulating the sail perturbation using a single horseshoe vortex and a self-preserved viscous plane wake.

The following three Figures, 19, 20, and 21 show the velocity distribution around the vortex cores. The results of the tangential velocity of the lifting line approach and the CFD simulations are compared for different setups with one or two sail rigs. The figures below show the results of the calculations with the 27° AoA and 0° heeled sail rig.
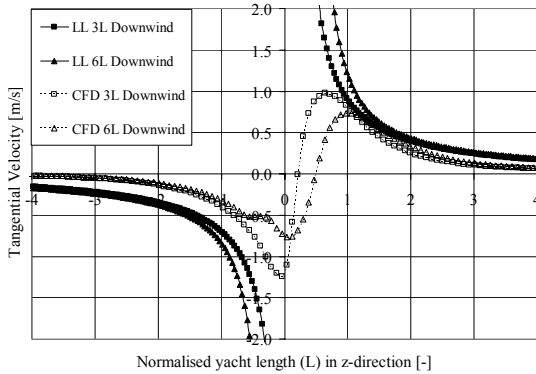

Figure 19. Velocity distribution (vortex flow) displaying the lifting line (LL) and the CFD

Figure 19 displays the tangential velocity distribution around the vortex core at *3L* and *6L* downstream of the sail rig using the lifting line approach and the CFD simulations (large extended domain). The lifting line results for both cases show good agreement with the CFD results for the port side of the vortex core (positive z-direction). On this side almost no difference between the different calculation methods can be seen for a distance of one and two yacht lengths away from the vortex centre. Further away from the vortex core a small overprediction of the lifting line approach is observed but still shows good agreement with the CFD results. An overprediction of the tangential velocity using the lifting line method can be seen for the starboard side of the vortex core (negative z-direction) which can be explained by the influence CFD results of the wind tunnel side wall.
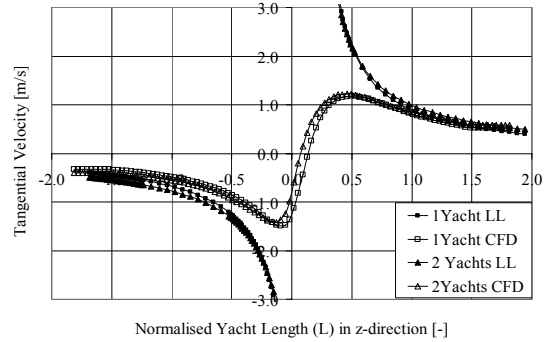

Figure 20. Two yachts setup: Velocity distribution (tangential velocity) in z-direction of the vortex core *2.5L* downwind of the sail rig;

Calculations of one sail rig and two sail rigs in-line with a distance of 3 sail rig lengths between them were carried out and the corresponding results are displayed in Figures 20 and 21. Figure 20 shows the tangential velocity at *2.5L* downstream of the upwind yacht using one and two sail rigs. Figure 21 also displays the results of one and two yachts by illustrating the tangential velocity *4L* downstream of the upwind yacht and one sail rig length downstream of the second yacht respectively. The influence of the second yacht is predicted by both calculations which results in a slightly higher tangential velocity around the vortex core. The predicted values of the lifting line method show good agreement with the CFD results, especially for distances further away than 1 sail rig length from the vortex core. It is worth pointing out that the model captures important flow details around the sail rig like the upstream influence of a yacht that was neglected in previous models like [3].
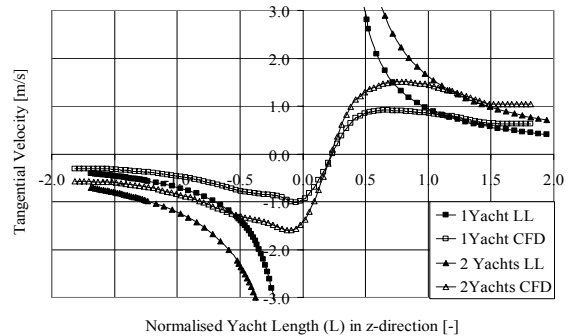

Figure 21. Two yachts setup: Velocity distribution (tangential velocity) in z-direction of the vortex core *4L* downwind of the sail rig; showing results of the lifting line approach and CFD.

Figure 21 shows the tangential velocity *4L* downstream of the upwind yacht considering one and two yachts respectively. The effect of the second yacht is visible due to an increased tangential velocity in both two yachts calculations. As seen before, a too little prediction of the tangential velocity by the lifting line calculation can be observed. A more accurate prediction of the tangential velocity for the vortex core's starboard side

(negative z-direction) is noticed for both downstream locations which can be explained by a smaller influence of the wind tunnel side walls on this vortex side.

6. CONCLUSIONS

A lifting line method capable of describing the phenomena of blanketing and covering within a yacht fleet race simulation environment with multiple yachts is described in this study. Detailed CFD analysis of a yacht's wake gave important insight in the flow behaviour, especially of the vortex core development downstream of a sail rig. Furthermore, CFD simulations with two in-line yachts were carried out to provide an initial value for the shed height of the line vortex and use of the total sideforce for the vortex strength. The lifting line approach was compared with the CFD results and showed good agreement for single and multiple yacht setups. Important physical features like the upstream influence of a yacht are captured by the approach at a very low computational cost. The lifting line method will now be enhanced to include the following features to allow implementation of the Matlab routines within Robo-Race. This will include the use of a vortex core model to represent the viscous region and spreading as seen in Figure 17 as well as decay with time.

References

1. Scarponi M. (2008) "Including Human Performance in the Dynamic Model of a Sailing Yacht: A Combined Ship Science – Behavioural Science Approach Towards a Winning Yacht-Sailor Combination", *PhD Thesis*, Università di Perugia, Italy.

2. Scarponi, M. & Shenoi, R. A. & Turnock, S. R. & Conti, P. (2007), "A combined ship science behavioural science approach to create a winning yacht-sailor combination", SNAME, *The 18th Chesapeake Sailing Yacht Symposium*, 1-10.

3. Philpott, A. & Henderson S. G. & Teirney, D. P. (2004), "A simulation model for predicting yacht match-race outcomes", *Operations Research*, **52**(1), 1-16.

4. Parolini, N. & Quarteroni, A. (2005), "Mathematical models and numerical simulations for the America's Cup", *Comput. Methods Appl. Mech. Engineering*, 194, 1001-1026.

5. Yoo, J. & Kim, J. & Park, I. & Ahn, H. & Van, S. (2006), "CFD Calculations on the Sail-like Three Dimensional Airfoils", *2nd High Performance Yacht Design Conference*, Auckland.

6. Spenkuch, T. (2006) "Effect of heel on sail rig performance using CFD: a quantified evolution of the ability of CFD to capture this behaviour", *MSc Thesis*, University of Southampton, UK.

7. Spenkuch, T. & Turnock, S. R. & Wright, A. M. & Shenoi, R. A. (2008), "The Use of CFD in Modelling Blanketing Effects for Yacht Race Simulations", *Numerical Towing Tank Symposium-NuTTS*, Brest, France.

8. Spenkuch, T. & Turnock, S. R. & Scarponi, M. & Shenoi, R. A. (2008), "Development of a sailing simulator environment for assessing and improving crew performance", *The Engineering of Sport,* 7, Springer, 65-76.

9. Masuyama, Y. & Kukasawa, T.& Sasagaw H. (1995), "Tacking Simulations of Sailing Yachts – Numerical Integration of Equation of Motion and Application of Neural Network Technique", SNAME, *Proceedings of the 12th Chesapeake Sailing Yacht Symposium*, 117-131.

10. Katz, J. & Plotkin A. (2001), *Low-speed Aerodynamics*, 2nd edition, Cambridge University Press, UK.

11. Teeters, J. & Ranzenbach, R. & Prince, M. (2003), "Changes to Sail Aerodynamics in the IMS Rule", *Proceedings of the 16th Chesapeake Sailing Yacht Symposium.*

12. Lesieur, M, & Begou, P. & Comte, P. & Métais, O. (2000) "Vortex recognition in numerical simulations", *ERCOFTAC*, Bulletin No. 46, 25-28.

13. Banks, D. & Singer, B. (1995) "A predictor-corrector technique for visualizing unsteady flow", *IEEE Transactions Visualization and Computer Graphics 1*, **1**, 151-163.

14. Collie, S. & Gerritsen, M. (2006), "The Challenging Turbulent Flow Past Downwind Yacht Sails and Practical Application of CFD to Them.", *2nd High Performance Yacht Design Conference*, Auckland.

15. Newman, B. & Low, H. (1984) "Two-dimensional impervious sails: experimental results compared with theory', *Journal of Fluid Mech.*, Cambridge University Press, **144**, 445-462.

16. Claughton, A. R. & Wellicome, J. F. & Shenoi, R. A. (2006), S*ailing yacht design: Theory*, 2nd edition, Addison Wesley Longman, Southampton, UK.

17. Roncin, K. & Kobus, J. M. (2004), "Dynamic simulation of two sailing boats in match racing", *Sports Engineering*, Springer London, **7**(3), 139-152.